Experiments and modelling of cavitating flows in Venturi. Part II: unsteady cavitation

Régiane Fortes-Patella, Stéphane Barre, Jean-Luc Reboud

Sixth International Symposium on Cavitation
CAV2006, Wageningen, The Netherlands, September 2006

EXPERIMENTS AND MODELLING OF CAVITATING FLOWS IN VENTURI
PART II: UNSTEADY CAVITATION

Regiane FORTES PATELLA - LEGI – INP Grenoble, France : fortes@hmg.inpg.fr
Stéphane BARRE - LEGI – INPG, France
Jean-Luc REBOUD - CNRS-LEMD, University of Grenoble, France

ABSTRACT

Some recent experimental and numerical studies were developed following previous works [Stutz et al. 1997b, 2000, Coutier 2004] and improving the physical analyses concerning unsteady behaviour of cavitating flows. Studies refer to a Venturi type section geometry characterized by a convergent angle of 18° and a divergent angle of about 8°. Recent experimental data are obtained by double optical probes measurements in cold water. A new method to treat experimental data, evaluate time-averaged values and standard deviations of the void fraction and the velocity field is proposed.

Numerical calculations were performed with the 2D cavitating unsteady code "IZ", by applying two homogeneous approaches: the barotropic model proposed by [Delannoy 1990] and the void ratio transport equation proposed by [Kunz 1999]. No-reflecting boundary conditions, simulating the hydroacoustic behaviour of inlet and outlet pipes of the Venturi test section, were implemented and used to simulate cavitating flows.

Unsteady local flow analyses were proposed from comparisons between experiments and simulations of unsteady cavitation in the considered Venturi geometry.

INTRODUCTION

The present study has been developed in parallel to the study presented in [Rolland et al., 2006]. It follows previous experimental and numerical studies carried out by the Turbomachinery and Cavitation team of LEGI (Grenoble, France) in order to better understanding and modelling the cavitation phenomena [Reboud et al., 1998, 2003, Coutier-Delgosha et al., 2004]. The works are led in collaboration with the French space agency (CNES) and the rocket engine division of Snecma.

The paper presents an experimental study and numerical calculations concerning unsteady cavitating flows in a Venturi geometry (named “Venturi 8°”).

Experimental facility and data processing are detailed in [Rolland et al., 2006]. They have been improved in relation to the studies previously presented by [Stutz 1997b, 2000] concerning the same geometry. In this paper, we present the main experimental results obtained for a given cavitation condition in the considered geometry. The results concern principally void ratio and flow velocity fields in cavitating zones.

The same developed data processing has been applied to treat numerical results obtained by unsteady simulations. The numerical code, described in detail by [Coutier et al., 2003a] and applied for different cavitating flow configurations in [Reboud et al. 1999][Lohrberg et al., 2002] [Coutier et al., 2002] [Fortes et al., 2006], has been developed in our team with the support of the CNES-Centre National d’Etudes Spatiales. The tool has been recently modified to improve physical modelling, boundary conditions and post-processing.

In this paper, we present main comparisons between experimental and numerical results obtained, as well as some analyses carried out for this Venturi geometry.

NOMENCLATURE

c_{mim}: minimum speed of sound in the mixture (m.s^{-1})
L_{ref}: geometry reference length (Venturi chord) = 0.224 m
p: local static pressure (Pa)
p_{inlet}: inlet pressure (Pa)
p_v: vapour pressure (Pa)
T_{ref}: reference time = $L_{ref}/ V_{ref} \approx 0.03$ s
V_{ref}: reference velocity= inlet velocity = 7.04 m/s
V : flow velocity (m/s)
α: void ratio $\alpha = \frac{(\rho - \rho_L)}{(\rho_V - \rho_L)}$ (-)
ρ: mixture density $\rho = \alpha\rho_V + (1-\alpha)\rho_L$ (kg.m^{-3})
$\rho_{l\,(=\rho_{ref})}$, ρ_v: liquid, vapour density (kg.m^{-3})

$\sigma_{inlet} = \frac{p_{inlet} - p_{vap}}{\frac{1}{2}\rho_{inlet} U_{inlet}^2}$ Cavitation number (-)

$Cp = \frac{p - p_{inlet}}{\frac{1}{2}\rho_{inlet} U_{inlet}^2}$ Pressure coefficient (-)

1. EXPERIMENTAL STUDY

1.a. Experimental conditions

In the present study, we use a Venturi profile with a convergence angle of 18° and a divergence angle of about 8°. This profile, illustrated in Figure 1, is characterized by the following geometrical data:

Inlet section: S_E = 50 X 44 mm² (where the reference pressure is measured);

Throat section: S_{throat} = 33.5 X 44 mm²;

Length of the test section (chord): L_{ref} = 224 mm.

The profile is equipped with four probe holes to take various measurements such as the local void ratio, instantaneous local velocity and pressure. Their positions X_I from the throat of the Venturi are:

X_1 = 13.7 mm; X_2 = 31.5 mm; X_3 = 49.9 mm; X_4 = 67.7 mm.

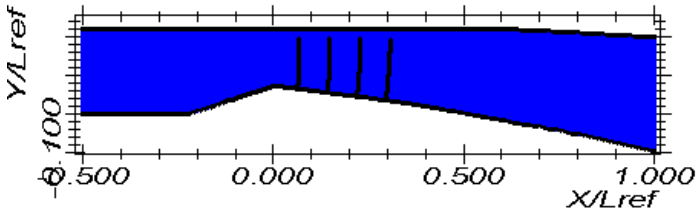

Figure 1: Schematic view of the Venturi profile and the probe positions.

The operation point of the hydraulic system is the same used by [Stutz 1997b and 2000]. It is characterized by the following physical parameters:

$V_{inlet} = V_{ref}$ = 7.04 m/s: inlet velocity (reference velocity)

Q = 0,0155 m^3/s: flow rate imposed in the hydraulic loop by the circulating pump

σ_{inlet} =2.15 ± 0,06: cavitation number at the inlet section.

According to experimental observations, with these parameters, the cavitating flow in this geometry is unsteady, with quasi-periodic fluctuations of attached sheet cavity and vapour clouds shedding. The maximum cavity length L is about 45 mm. The vapour shedding frequency is near to 45 Hz estimated from FFT analysis of unsteady pressure signal or visualizations under stroboscopic light.

The most important differences with respect to previous work [Stutz 2000] are:

- the double optical probe used to evaluate void ratio and velocity fields. We use an optical probe made of two sapphire optical fibers of 80 µm diameter and with frayed ends. The inter-tips distance is 1,05 mm ± 0,02. In previous work, the inter-tips distance was about 2 mm. The optical probe previously used was constituted of two glass fibers with a 0.025 mm tip radius. This characteristic caused a lot of breaking probe problems due to the aggressiveness of the unsteady flow studied.

- data acquisitions are carried out on a fast A/D data acquisition board NI-DAQ PCI-6110E. For each acquisition we record 4 million points per way (one way by optical probe), with a sampling rate of 100 Khz (either a time of 40 seconds acquisition per measurement). For each Y position of the optical probe in the Venturi (between ten and fifteen per station), hundred successive measurements are taken. It generates 400 million points of measurement per position in the cavity corresponding to an observation time of 4000 s. This was absolutely necessary because of the method used to obtain instantaneous velocities values: it is based on the determination of the convective velocity of some selected bubbles being respectively detected by the two probes [see Rolland et al. 2006 for details]. In the studied flow, the void ratio is particularly low (between 1 and 10% depending on the probed station). So, for a given observation time, the number of detected bubbles is very low. Furthermore, the velocity calculation algorithm rejects a lot of bubbles and then only about 10% of the detected bubbles are validated to give a useable velocity value. This very high observation time (compared to about 0.45 million data in 6 s per probe position recorded and treated in previous study) was used to obtain sufficiently converged statistics, which allow us to perform, in the near future, an unsteady phase averaging analysis. This quite important effort (about 5 Gigabytes of raw data for each probed positions in the flow) may lead us to obtain sufficiently averaged statistics even in the case of a high-resolution phase averaging process. Works are in progress to describe precisely the overall dynamics on the flow inside the cavitation sheet.

According to experimental observations, cavitation sheets develop from the Venturi throat and show typical self-oscillation behaviour, with quasi-periodic vapour clouds shedding. For the estimated inlet cavitation number σ of about 2.15 ± 0.06 (based on the time-averaged upstream pressure ≈ 55000 Pa) and an inlet velocity V_{ref} = 7.04 m/s, the cloud shedding frequency observed experimentally is about 45 Hz (≈1.4 V_{ref}/L_{ref}) for a maximum attached cavity length of 45mm (≈0.2 L_{ref}).+/- 5mm. That gives the classical Strouhal number, based on the cavity length: St ≈ 0.3.

1.b. Estimation of the local void ratio

The local void ratio α of a gas/liquid mixture is defined here as the ratio between the cumulated attendance time of the gas phase and a given time of observation, in a point of the flow. It is given by:

$$\alpha = \frac{\sum_{i=1}^{n} T_{vap\_i}}{T_{tot\_obs}}$$

The post-processing algorithm enables us to exploit the signal from the optical probe, by distinguishing the gas phase from the liquid phase according to the value of the measured tension. The maximum value V_{max} corresponds to the vapour state, and the minimal value V_{min} to the liquid state. In order to

estimate the local void ratio, we must fix a threshold in tension $V_{threshold}$. It allows to determine the phase of the fluid around the probe: liquid state if $V < V_{threshold}$, and gas state if $V > V_{threshold}$. This threshold is fixed according to the parameter:

$$\beta = \frac{V_{threshold} - V_{\min}}{V_{\max} - V_{\min}}$$

The value of this parameter was gauged in great detail for this type of flow by [Stutz et al. 1996, 1997a, 1997b, 2000, 2003]. They retained a value of $\beta = 0.1$ to give correct void ratios for this typical flow pattern. We used this value for the determination of the void ratio. For more details about the void ratio determination, see [Rolland et al. 2006].

1.c. Estimation of instantaneous local velocity

The determination of the local velocity is based on the method detailed in [Rolland et al. 2006]. Some minor adaptations were used here by reducing the β_{high} threshold to a value of 0.54 instead of 0.8, which has been used in [Rolland et al. 2006]. Using this new value, we obtain a substantial increase of the detected bubbles population without any degradation of the quality of the velocity field determination [Rossi 2004].

By processing the instantaneous velocity values in the same way as detailed in [Rolland et al. 2006], we obtain, for each probed position, the Probability Density Function (PDF) of the local velocity field for the used observation time (4000s). A typical example, corresponding to the point Y=6mm for X_2=31.5mm probed position, is presented on Figure 2.

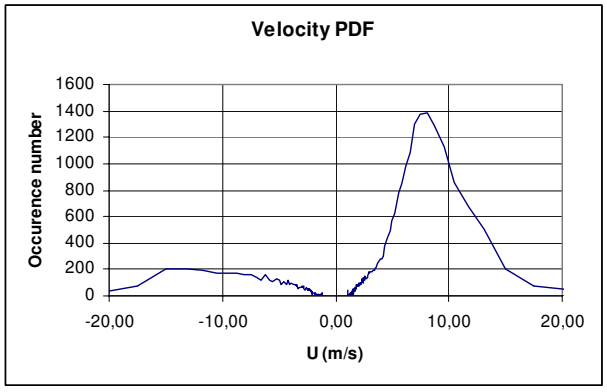

Figure 2: Velocity PDF for Y=6mm at X_2=31.5mm

From these data, we are able to describe the velocity field inside the cavity. For each point, we choose to keep the most probable value of the PDF to define the local velocity.

Experimental results obtained for flow velocity and void ratio fields have been confronted with ones evaluated by numerical simulation. Main results and analyses are presented here above.

2. PHYSICAL AND NUMERICAL MODELS

2.a. Numerical code

Calculations have been done with the 2D unsteady code "IZ", which has been developed in our team with the support of the CNES-Centre National d'Etudes Spatiales. Reynolds Averaged Navier-Stokes equations are solved for a homogeneous fluid with variable density:

$$\frac{\partial \rho_m}{\partial t} + \nabla.\left(\rho_m \mathbf{u}_m\right) = 0$$

$$\frac{\partial \rho_m \mathbf{u}_m}{\partial t} + \nabla.\left(\rho_m \mathbf{u}_m \otimes \mathbf{u}_m\right) = -\nabla(p_m) + \nabla.(\bar{\bar{\tau}}_m)$$

where $\bar{\bar{\tau}}_m$ is the shear stress tensor, , and ρ_m is the mixture density, defined with respect to the void ratio α as:

$$\rho_m = \alpha\ \rho_v + (1-\alpha)\rho_L$$

Applications concern cold water. Calculations do not take into account thermodynamic effects and the energy equation is not solved. Two phases are considered to be locally (in each cell) in dynamic equilibrium (no drift velocity). Each pure phase is considered incompressible.

A finite volume spatial discretization is applied in curvilinear orthogonal coordinates on a staggered mesh. An iterative resolution based on the SIMPLE algorithm was developed to deal with quasi-incompressible flow (α=0 and α = 1) and highly compressible flow (0< α <1) [Delannoy and Kueny 1990]. The liquid–vapour interfaces are described by high gradients of the mixture density ρ_m (hereafter also simply denoted ρ), which was allowed by using a conservative approach and the HLPA no-oscillatory second order MUSCL scheme proposed by [Zhu, 1991].

To solve the time-dependant elliptic problem, first or second order fully implicit methods are available. A complete description of the numerical scheme is presented by [Coutier et al, 2003a].

Turbulent flows are calculated by solving the Reynolds equations using a modified k-ε RNG turbulence model with standard wall functions. The modified k-ε RNG turbulence model is described in detail in [Coutier et al., 2002, 2003b].

2.b. Barotropic Model

To model cavitation phenomenon and to close the governing equations system, a barotropic state law has been firstly used. The fluid density (and so the void fraction) is controlled by a law $\rho(p)$ that links explicitly the mixture fluid density to the local static pressure. This law is mainly controlled by its maximum slope, which is related to the minimum speed of sound c_{min} in the mixture. This model was widely described in previous works [Coutier et al., 2002, 2003a,b]. An illustration of the barotropic law is given in Part I [Rolland et al., 2006].

Recent numerical tests allowed to better estimating the influence of c_{min} and ρ_v/ρ_l parameters on unsteady cavitating results. Table 1 gives physical parameters

applied for numerical tests. Main results are presented in section 4 of the paper.

ρ_v/ρ_ℓ	c_{min} *m/s*
0,001	1 1.5 2
0,00003	1

Table 1: Physical parameters applied

2.c. Void ratio transport equation

Based on the work proposed by [Kunz et al., 1999], another physical model has been implemented in the "IZ" code. It consists in solving a "transport equation for the void ratio". As a matter of fact, the transport equation is derived from mass equations for vapour phase and liquid phase:

$$\frac{\partial \alpha \rho_V}{\partial t} + \nabla \cdot (\alpha \rho_V U) = -(\dot{m}_{VL} + \dot{m}_{LV}) \qquad (1)$$

$$\frac{\partial (1-\alpha)\rho_L}{\partial t} + \nabla \cdot ((1-\alpha)\rho_L U) = (\dot{m}_{VL} + \dot{m}_{LV}) \qquad (2)$$

which include empirical terms $\dot{m}_{VL}$ and $\dot{m}_{LV}$ for vaporization and condensation phenomena. If we consider ρ_v and ρ_ℓ constants, we can deduce from (1) the transport equation:

$$\frac{\partial \alpha}{\partial t} + \nabla \cdot (\alpha U) = -\frac{1}{\rho_V}(\dot{m}_{VL} + \dot{m}_{LV})$$

In the present work, we apply:

$$\dot{m}_{LV} = C_{LV} \cdot \rho_L (1-\alpha) \mathrm{Min}(0, Cp + \sigma) / \tau$$

$$\dot{m}_{VL} = C_{VL} \cdot \rho_L \alpha (1-\alpha)^2 / \tau$$

where τ is a characteristic time, and C_{LV}, C_{VL} are empirical constants.

To treat the strong variations of mixture density by applying the pressure-correction method proposed by [Patankar, 1981], an estimation of the term $d\rho/dP$ is required. In the case of the barotropic model, this term is directly deduced from the state equation. In the case of the void ratio transport equation approach, the term $d\rho/dP$ is deduced from the vaporization term by:

$$\frac{d(\rho/\rho_l)}{dCp} = \frac{\rho_l}{\rho_v} Cvap \cdot Min((1-\alpha), \alpha)(dt/T_{ref})$$

where $Cvap = C_{LV}\, Tref / \tau$, dt is the time step, Cp is the pressure coefficient and Tref is the reference time.

In the present study, we have considered:

$\rho_v/\rho_l = 10^{-3}$, $Cvap = 0.2$ and $Cond = C_{VL}\, Tref / \tau = 0.05$

3. GEOMETRY AND BOUNDARY CONDITIONS

3.a. Grid

To study the Venturi geometry presented in Section 1, we have used a computational grid composed of (173 x 61) orthogonal cells (Figure 3). A special contraction of the mesh is applied in the main flow direction just after the throat in order to better simulate two-phase flow area. In the other direction, to use standard laws of the walls, a contraction is also applied close to the walls to obtain, at the first grid point, the dimensionless parameter y^+ of the boundary layer varying between 30 and 50 under no-cavitating conditions. The grid is finer in the bottom part of the Venturi section than in its upper part, to enhance the accuracy in the cavitation zone.

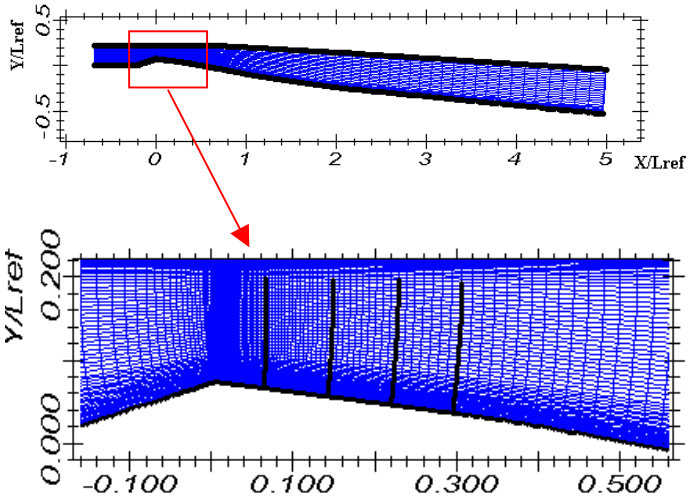

Figure 3: Curvilinear- orthogonal mesh of the Venturi type section (173x61 cells). L_{ref} =224 mm

3.b. Boundary conditions

In previous studies, we applied classical boundary conditions; i.e., the mass flow rate was imposed constant as upstream boundary condition, and static pressure was imposed as downstream boundary condition allowing the control of the outlet cavitation number σ_{outlet}.

This kind of boundary conditions impedes an appropriate comparison between measurements and calculations, mainly for unsteady cavitating flows. Indeed, in experiments, the reference pressure is measured at inlet section of the Venturi and reference cavitation number is σ_{inlet}. In previous work, the comparisons between experiments and calculations results were carried out by adjusting *a posteriori,* by trial and error, the time-averaged value of numerical σ_{inlet} (obtained for a given imposed σ_{outlet}) to the experimental σ_{inlet} mean value.

Moreover, according to our previous studies, this type of boundary conditions tends to over-estimate the magnitude of pressure fluctuations [Reboud et al., 1999].

In order to improve boundary conditions, the code "IZ" was modified to take into account circuit impedance and to permit to use no-reflecting boundary

conditions [Pouffary et al., 2004]. Figure 4 illustrates the scheme applied.

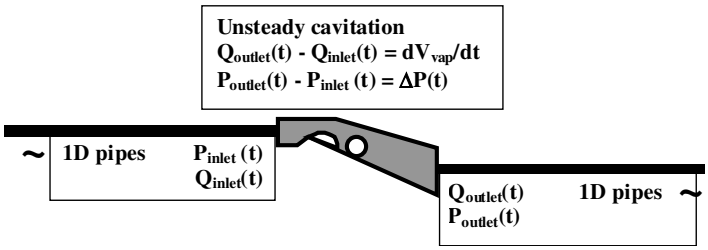

Figure 4: Coupling between 3 considered domains: cavitation tunnel, upstream and downstream pipes

The circuit impedance is modelled by a 1D hydro-elastic model that solves the Allievi's equations [Longatte, 1998]. No-reflecting boundary conditions [Thompson, 1987, 1990] are applied at one end of each pipe. The other end is coupled with the 2D computational domain of the cavitation tunnel.

Inlet and outlet boundary conditions applied to the Venturi geometry are modified in function of pipes hydro-elastic behaviour. So, at each time step, an iterative procedure allows coupling the inlet/outlet flow rates and pressures with respect:

- to the cavitation behaviour in the Venturi test section; i.e. to the pressure and vapour volume fluctuations due to the cloud shedding process,
- and to the propagation of pressure and flow rate fluctuations in the pipes (Figure 4).

Making use of this pipes/Venturi coupled calculations, we can control and impose the mean values of flow rate and σ_{inlet} during numerical simulations. These mean values are estimated and corrected during the computation by time averaging of slow variations of inlet pressure and flow rate (i.e. variations corresponding to a characteristic time much larger than the cavitation cycle period).

For results presented in this paper, we have considered pipes characterized by a diameter of 0.12m and a sound celerity of 1000 m/s (pipes length has no influence because of the no-reflecting condition applied).

3.c. Transient conditions

To initialise cavitating numerical calculations, the static pressure imposed as downstream boundary condition is slowly decreased from a high value leading to steady no-cavitating conditions, down to a value required to assure the expected mean cavitation number σ_{inlet}. Phase change then occurs spontaneously in the regions where the pressure decreases close to the vapour pressure Pv.

4. COMPARISON BETWEEN EXPERIMENTAL AND NUMERICAL RESULTS

4.a. Calculation Conditions

The studied case, presented in Section 1, leads to an unsteady cavitation sheet with a maximum length of about 45 mm, with V_{inlet}=7.04 m/s and experimental σ_{inlet} of 2.15 ± 0.06.

In order to simulate this unsteady cavitating flow, many calculations have been performed by considering different physical models, parameters and σ values.

Some numerical tests, summarized in Table 2, provided global results near to experimental ones.

The reference density is the liquid density equal to 998 kg/m^3. Time step is dt=0.01Tref and simulation duration is about 6s (200 Tref) for all the tested cases.

case	model	c_{min} (m/s) or (cvap; cond)	ρ_v/ρ_ℓ	σ_{inlet} *mean value*	σ_{inlet} *most probable value*	σ_{outlet} *mean value*	L_{cav} (/Lref)	f (hz)	vapour volume (/Lref^3) *mean value*	vapour volume (/Lref^3) *standard deviation*
1	barotropic	1	0.001	2.3	~2.1	2.73	~0.18 (40mm)	~45	$1.0\ 10^{-3}$	$7.2\ 10^{-4}$
2	barotropic	1	$3\ e^{-5}$	2.3	~2.1	2.75	~0.2 (45mm)	~45	$8.6\ 10^{-4}$	$5.9\ 10^{-4}$
3	barotropic	1.5	0.001	2.3	~2	2.67	~0.19 (43mm)	~45	$1.64\ 10^{-3}$	$9.4\ 10^{-4}$
4	barotropic	2	0.001	2.4	~2.1	2.8	~0.2 (45mm)	~40	1.1710^{-3}	$2.5\ 10^{-4}$
4a	barotropic	2	0.001	2.3	~1.9	2.31	~0.7 (160mm)	~15	$2.28\ 10^{-2}$	$8.9\ 10^{-3}$
5	Void ratio equation	0.2 0.05	0.001	2.6	~2	2.94	~0.23 (51mm)	~35	$1.2\ 10^{-3}$	$5.5\ 10^{-4}$
[ref]	barotropic	1.5	0.001	2.4	-	2.8	~0.19	55	$1.38\ 10^{-3}$	$2.4\ 10^{-4}$

Table 2: Tested cases. "L_{cav}" is the maximal attached cavity length; "f" is the vapour shedding frequency [ref] : previous results presented in [Coutier et al., 2004]

4.b. Global Analyses

Tests have been conducted to obtain almost the same maximal sheet length. According to our study, the representative parameter of unsteadiness of cavitating flow seems to be the *most probable value of* σ_{inlet}. For all performed tests, this value had to be approximately 2 – 2.1 in order to obtain cavitating flow behaviour near to one observed experimentally. It is interesting to note that the obtained numerical σ_{inlet} most probable value is very near to experimental σ_{inlet} value. As a matter of fact, experimental σ_{inlet} value fluctuates during experiments and further work is required to characterize the magnitude and the frequencies of these fluctuations.

During this numerical study, we have observed that the time-averaged value of σ_{inlet}, which was used in previous work as reference value, did not represent the unsteady behaviour of cavitating flow. Indeed, we can observe the same unsteady behaviour (corresponding to a similar most probable value of σ_{inlet}) and different σ_{inlet} time-averaged values (see cases 1, 4 and 5). Vice versa, we can observe different unsteady behaviours obtained for a same σ_{inlet} time-averaged value (see cases 3 and 4a, for example).

By comparing global results obtained for cases 4 and 4a, we observe a strong modification of the simulated unsteady behaviour due to a slight mean σ_{inlet} variation: $\sigma_{inlet} = 2.3$ leads to a Lcav of about 160mm and a shedding frequency near to 15 hz, while $\sigma_{inlet} = 2.4$ leads to a Lcav of about 45mm and a shedding frequency near to 40 hz. This high sensibility of the unsteady cavitating flow to the σ_{inlet} variation has been also observed during experiments for the σ_{inlet} range analysed.

Three computations with different c_{min} values have been compared for a given ratio $\rho_v/\rho_l = 10^{-3}$ (see cases 1, 3 and 4). Concerning global results presented in Table 2, slight variations of cavity length and shedding frequency are observed. The influence of c_{min} on the mean total vapour volume and standard deviation does not show a clear tendency.

Results indicate also similar global behaviour obtained for ratios $\rho_v/\rho_l = 10^{-3}$ (case 1) or $\rho_v/\rho_l = 3.10^{-5}$ case 2). Some local analyses presented here below allow to an improved comparison between tested parameters.

These complementary analyses concern local void ratio and velocity profiles comparisons inside the cavity. Experiment results have been obtained for two stations corresponding to the distances $X_1 = 13.7$ mm and $X_2 = 31.5$ mm from the Venturi throat. Numerical results correspond to the distances $X_1 = 13.7$ mm; $X_2 = 31.5$ mm; $X_3 = 49.9$mm and $X_4 = 67.7$ mm.

4.c. Flow velocity fields

Figures 5, 9 and 10 show the evolutions of the longitudinal velocity obtained from recent experiments (corresponding to the most probable value of the velocity at each probe position) and computations (corresponding to the time averaged value of the velocity at each probe position). Numerical results concern different tests presented in Table 2. The corresponding standard deviation results are illustrated in Figures 6.

Globally, in a qualitative point of view, the performed unsteady simulations seem to describe correctly the periodic re-entrant jet observed experimentally. According to numerical calculations, for stations 1, 2 and 3, we observe a recirculating flow corresponding to a re-entrant jet that extends roughly one third of the sheet thickness. The presence of the re-entrant jet is characterized by negative or zero mean values of the velocity close to the wall. For station 4, the obtained mean velocity profiles are close to one observed in a classical turbulent boundary layer without recirculation.

By comparing cases 1 and 5, we observe different results concerning mainly the stations 1 and 3: with void ratio transport equation model (case 5), the mean velocity deficit obtained near to the wall is smaller in station 1 and higher in station 3 in comparison with barotropic approach.

We do not notice a high influence of the applied model on the magnitude of velocity standard deviations: the fluctuations are associated to the presence of a re-entrant jet and to the convection of vorticity structures downstream of the cavitation sheet (see Figures 7 and 8).

Figures 9 and 10 compare some simulation and experimental results: for analysed data, it appears that barotropic model well predicts the thickness of re-entrant jet (near to 1.5 mm at station 1). By comparisons with recent experiments, simulations seems to underestimate the velocity deficit in the zone of the re-entrant jet.

To improve the unsteady aspect of the analysis we decided to focus on numerical results concerning station 1 at Y=2 mm in order to show a statistical analysis of the instantaneous velocity field. Results have been treated by the same data processing applied for experimental results (see section 1 of the paper). We particularly focused on instantaneous velocity PDF. Figure 11 shows these functions for the five computations done at the studied point (Y=2 mm at station 1). The first three cases show a good global qualitative agreement. We only have a single peak value per PDF. The most probable values are -0.6m/s for case 1; -0.98m/s for case 2 and -0.33m/s for case 3. In case 3 the peak seems thinner than in the two previous cases. This corresponds to a more organized solution for the velocity field with less almost random contribution coming from positive velocity solutions. Case 4 has a very different behaviour exhibiting three peaks. The two first ones are almost centred on zero value (-1.26m/s and 1.36m/s) and may correspond to an alternate fluctuation of the flow close to a sinusoidal solution for the velocity field. The third one (9m/s) may corresponds to the external velocity of the liquid flow surrounding the cavitation sheet. This peak is probably linked to external liquid flow incursions for some particular phases of the sheet pulsation cycle. Case 5 has a very different behaviour. No negative velocity solution was found. We can notice two peaks at 0.72m/s and 9m/s. Between these two peaks, the velocity population is very low. In this situation, the flow seems triggered and the velocity field is maybe close to an asymmetric square wave function.

a) time-averaged velocity (m/s): station 1

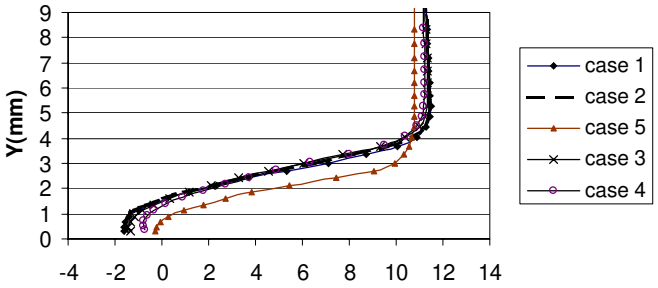

b) time-averaged velocity (m/s): station 2

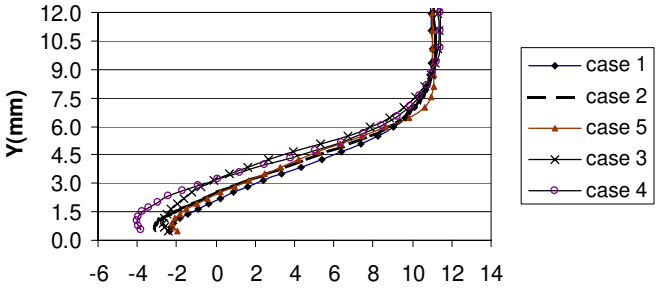

c) time-averaged velocity (m/s): station 3

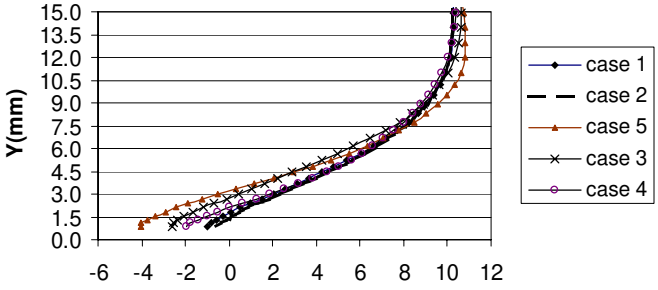

d) time-averaged velocity (m/s): station 4

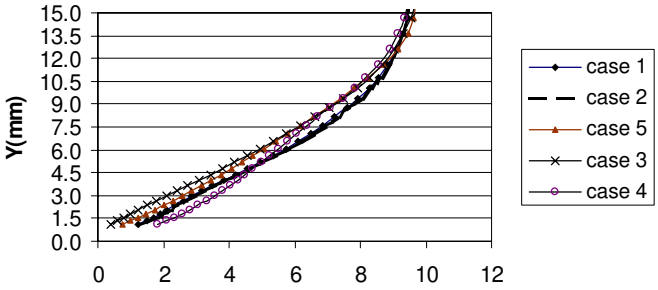

Figure 5: Time-averaged velocity profiles: Comparison between tests simulated

a) velocity standard deviation (m/s): station 1

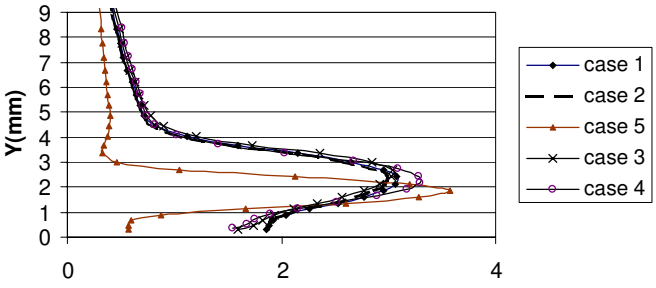

b) velocity standard deviation (m/s): station 2

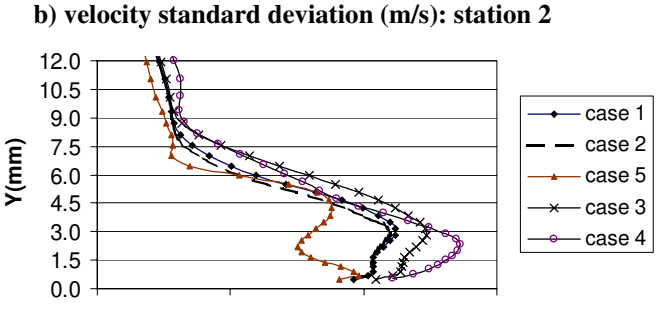

c) velocity standard deviation (m/s): station 3

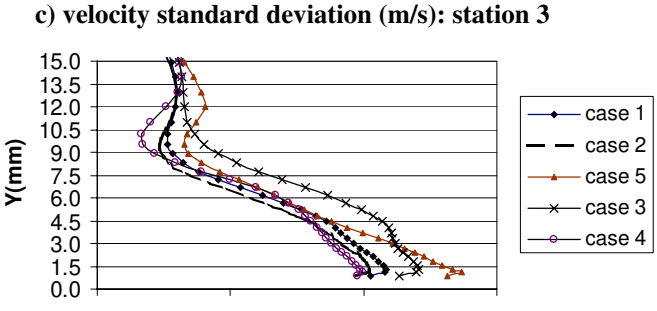

d) velocity standard deviation (m/s): station 4

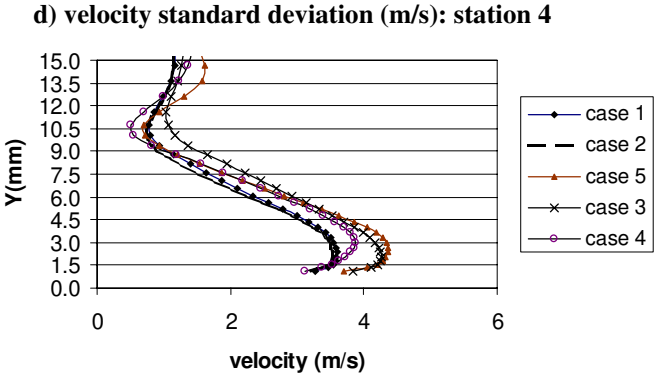

Figure 6: Standard deviation values of velocity Comparison between tests simulated

It is worth noting that for cases 1, 2, 3 and 4 the time averaged velocity at station 1, Y=2 mm, is close to 2m/s, exhibiting a quasi-perfect agreement (Figure 5a). This agreement is not confirmed by unsteady analysis, which clearly shows two classes of solution (Figures 11).

Velocity PDF obtained from experimental measurements is given in Figure 12. Result concerns position Y=2.5 mm at station 1. According to this first comparison, qualitative good agreement is obtained with the case 4 simulated. Further analysis works are in progress to improve these initial comparisons concerning unsteady results.

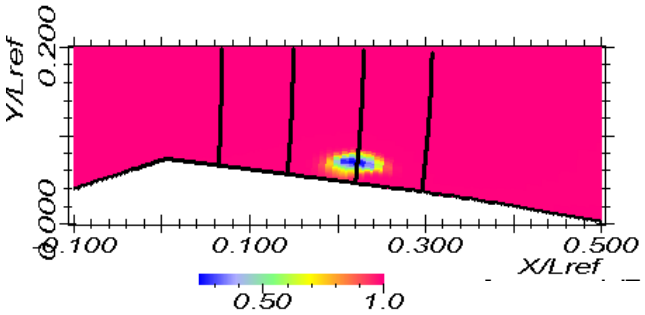

a) t = 58.8 Tref (case 5)

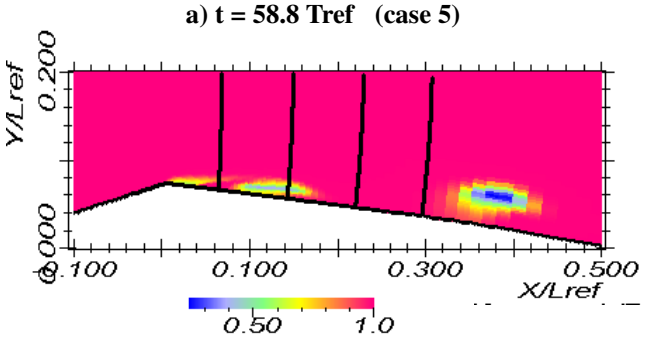

b) t = 58.2 Tref (case 5)

Figure 7: Density fields

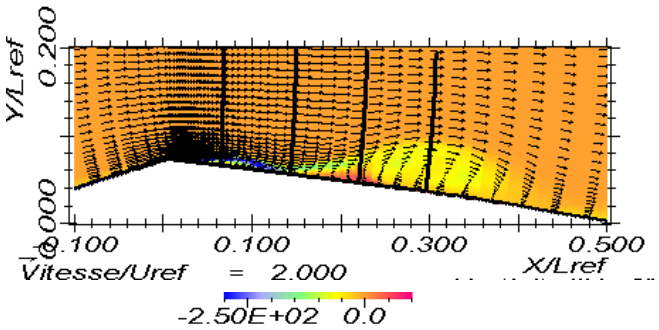

a) t = 59 Tref (case 5)

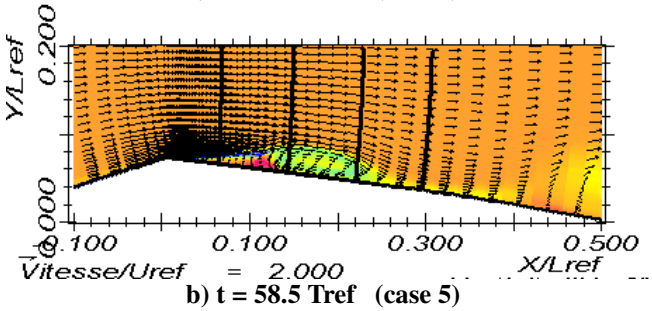

b) t = 58.5 Tref (case 5)

Figure 8: Vorticity and flow velocity fields

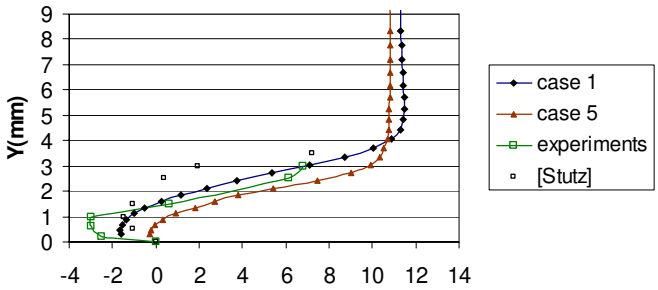

Figure 9: Velocity profiles: Comparison between calculations (time-averaged values), recent experiments (most probable values) and results presented by [Stutz, 1997a,b].; station 1

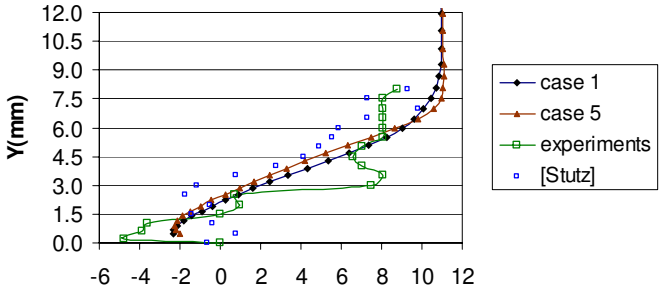

Figure 10: Velocity profiles: Comparison between calculations (time-averaged values), recent experiments (most probable values) and results presented by [Stutz, 1997a,b]; station 2

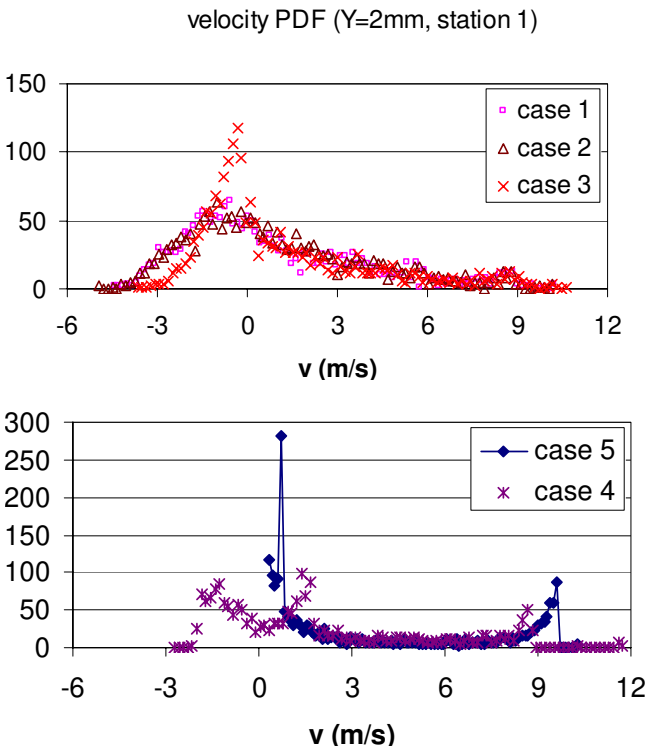

Figure 11: Velocity PDF: Comparison between tests simulated. Y=2mm, station 1

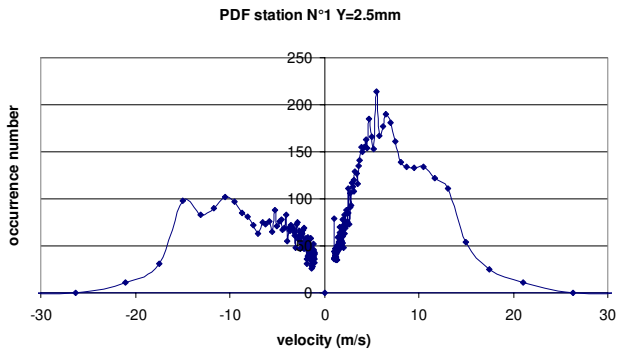

Figure 12: Velocity PDF: Experimental results. Y=2.5mm, station 1

4.d. Void ratio

Figures 14 and 15 illustrate numerical results concerning void ratio: time-averaged values and standard deviation. The influence of the physical models and parameters is here noticeable.

Concerning the sheet thickness, cases 1, 2 and 5 lead to a good agreement with experimental observations (Figures 13 and 14). Higher values of c_{min} (i.e. $c_{min} > 1$ m/s) cause an overestimation of cavity thickness.

For stations 1 and 2, the void ratio transport equation model (case 5) gives smaller values of time-averaged void ratio if compared to barotropic approach. For station 4, the tendency is opposite. For station 1, the simulated mean void ratio magnitudes obtained in case 5 are close to ones evaluated by experimental study. For station 2, this value is overestimated by numerical calculations. Globally, we observe low mean void ratio in the main part of cavitation sheet: it does not exceed 20% (according to case 5). For barotropic approach, this value can reach 30% in station 2.

The sheet thickness increases from station 1 to 4. Void ratio simulated in stations 1 and 2 seems to be related to unstable attached cavity (Figure 7b). Behaviours described in stations 3 and 4 are attributed to the passage of shed cavitation structures (Figure 7a).

We observe also high fluctuations of void ratio in stations 2 and 3 (Figures 15b and 15c).

5. UNSTEADY FLOW ANALYSES

5.a. Density fields

Figures 16 and 17 show density fields obtained during a cloud shedding period for cases 1 and 5. The characteristic period obtained from barotropic model is about 0.75 Tref . The void ratio transport equation model leads to a characteristic period of ~0.9 Tref.

The qualitative general behaviour is similar in both cases analysed: a cavity attached to the Venturi throat takes form and increases during the first half of the period. The attached sheet is broken by a re-entrant jet and a mixture vapour/liquid structure is shed. This structure is characterized by high instantaneous void ratios and by a significant vorticity field (see Figure 8). The convection of this structure by the main flow is associated to the development of a new attached cavity, which increases until the convected vapour structure collapses downstream. The implosion of this structure lead to the development of a new re-entrant jet and the cycle repeats oneself.

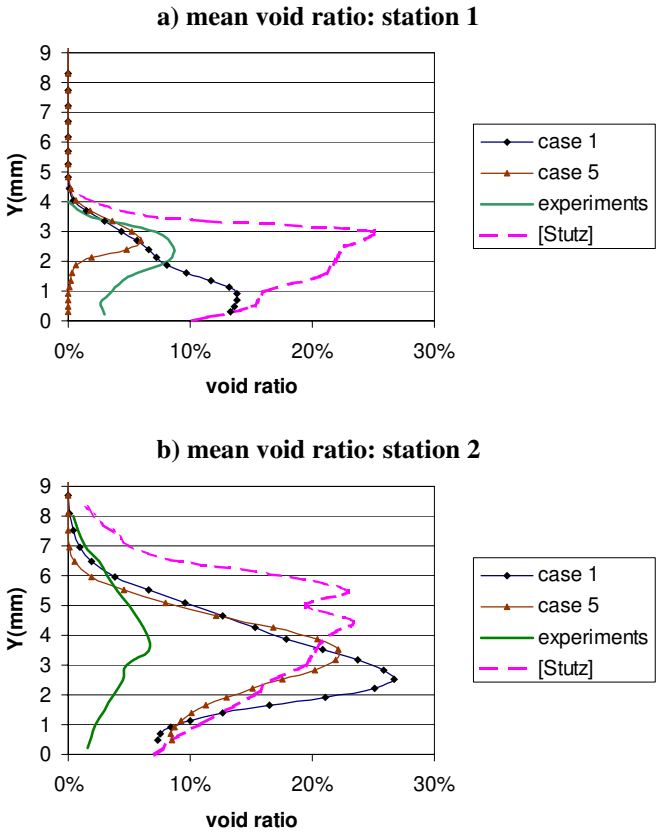

Figure 13: Time-averaged void ratio profiles: Comparison between calculations, recent experiments and results presented by [Stutz, 1997a,b].

5.b. Vapour volume variation

More significant discrepancies between both models are observed on total vapour volume fluctuations simulated (Figures 18 and 19).

We can observe that results obtained by case 5 are more stable and regular than ones concerning case 1. The magnitude of vapour volume fluctuations are close in both cases, but the unsteady behaviour obtained by the barotropic model seems to be characterized also by another frequency corresponding to a half of the shedding frequency. Further analyses are in progress to analyse and to better understand this behaviour.

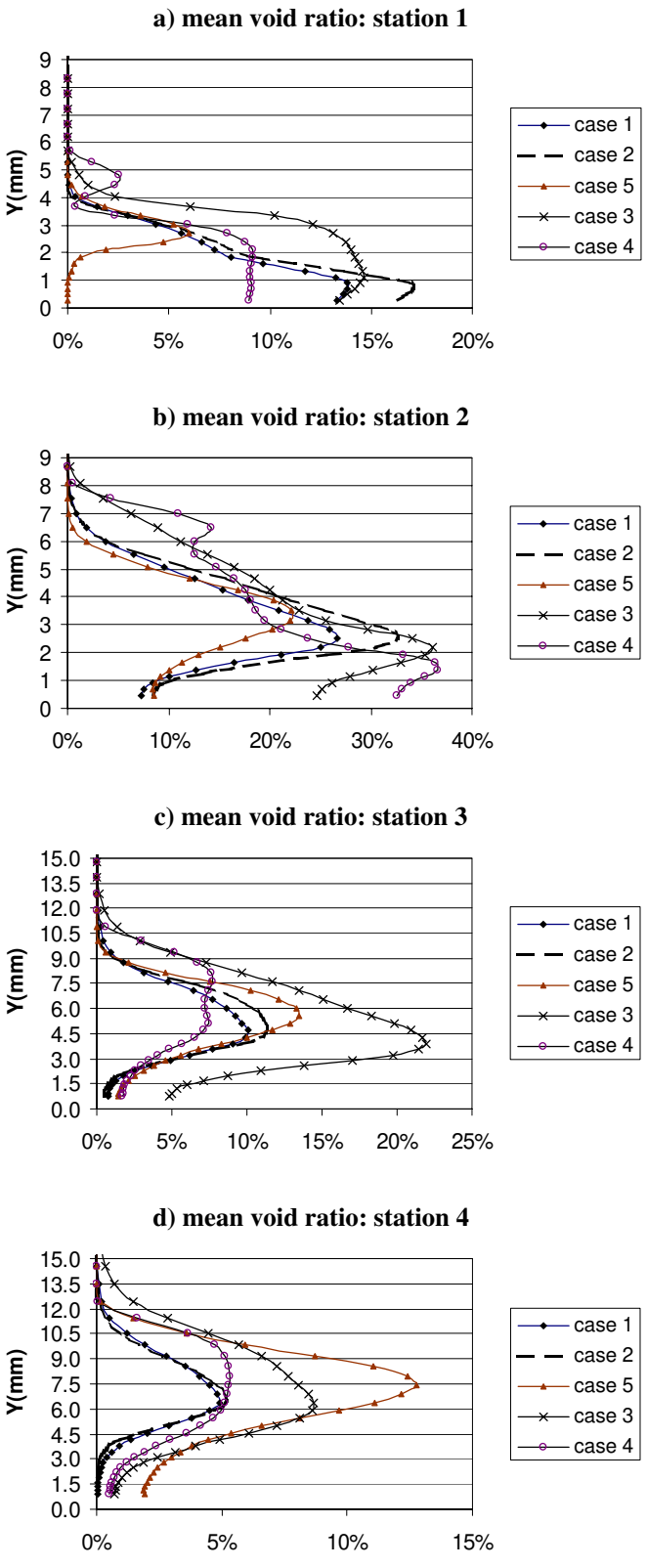

Figure 14: Time-averaged void ratio profiles: Comparison between tests simulated

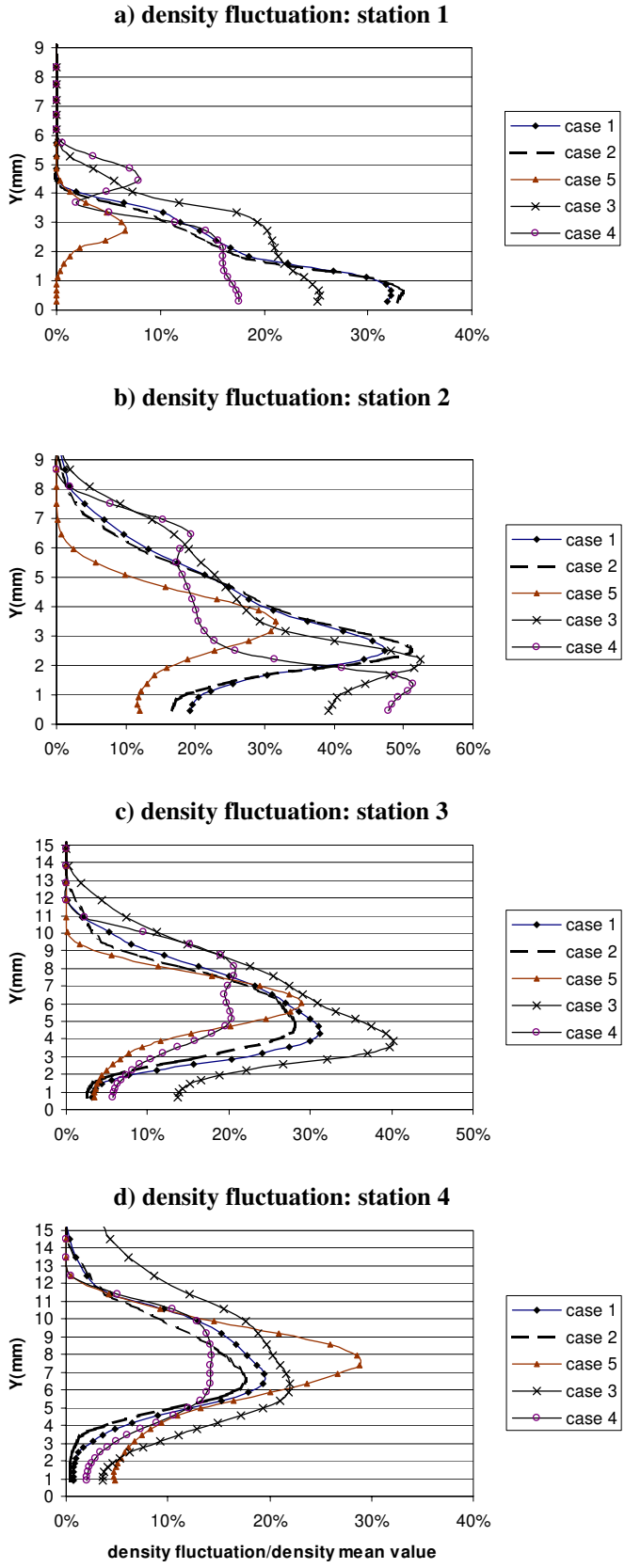

Figure 15: Standard deviation values of density (given as a proportion of the density mean value) Comparison between tests simulated

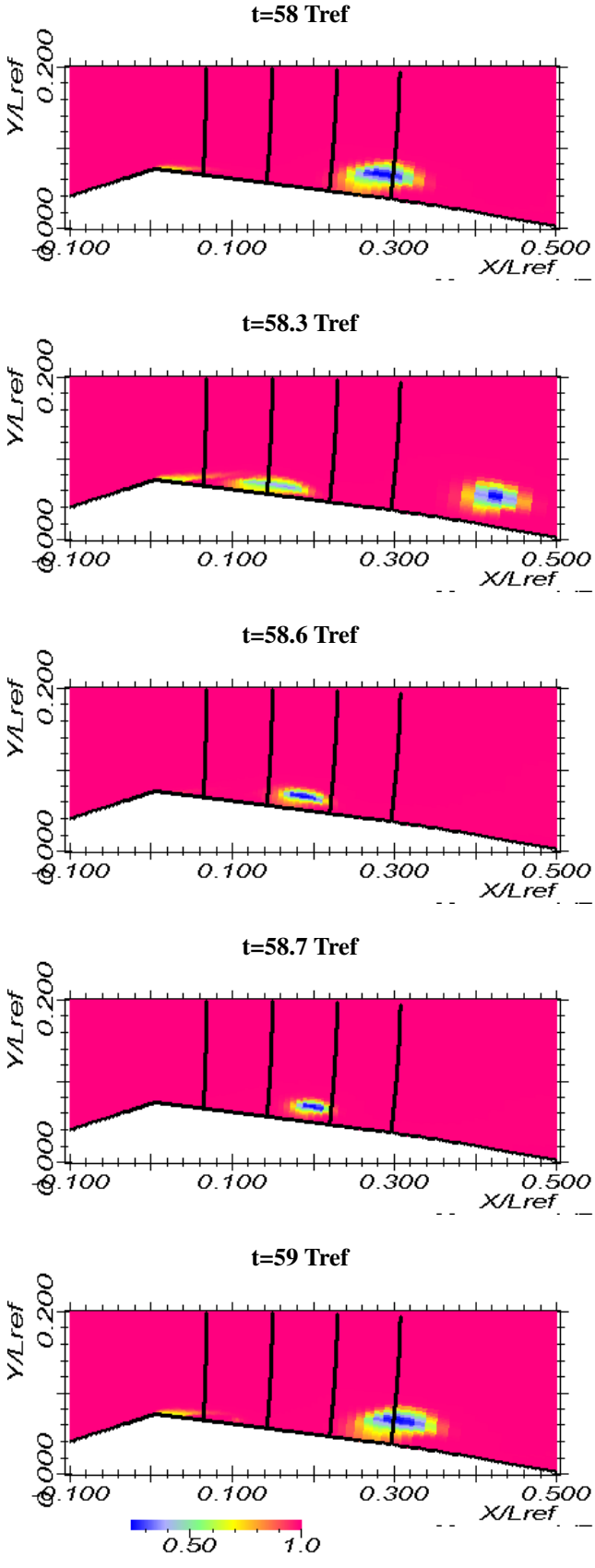

Figure 16: Density fields (case 5)

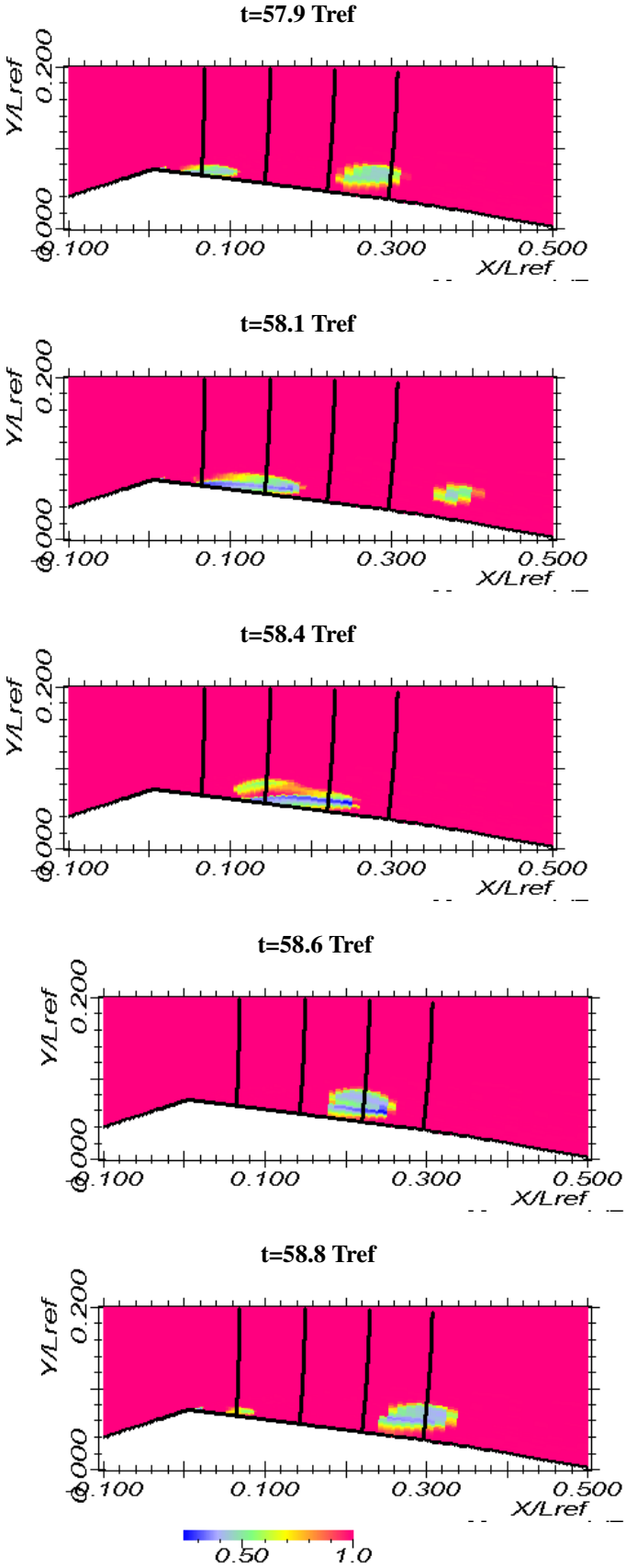

Figure 17: Density fields (case 1)

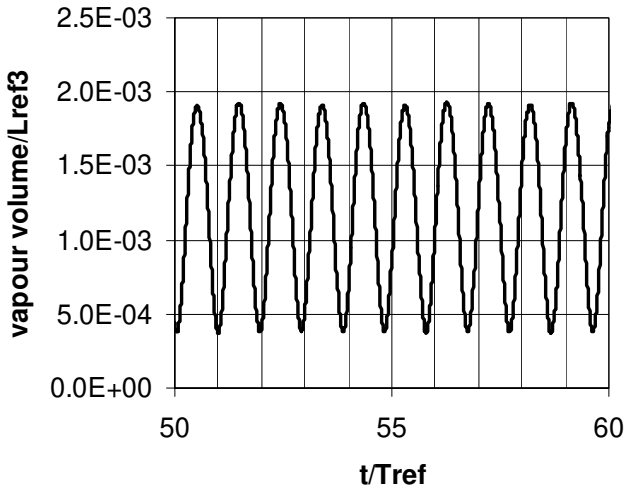

Figure 18: Dimensionless vapour volume fluctuations obtained with void ratio transport equation model (case 5). The vapour volume is divided by L_{ref}^3.

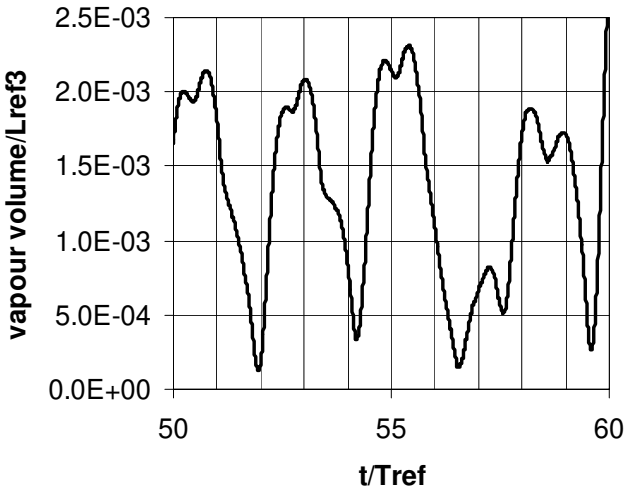

Figure 19: Dimensionless vapour volume fluctuations obtained with barotropic model (case 1). The vapour volume is divided by L_{ref}^3.

5.c. Head losses

In order to study the influence of the unsteady cavitation on head losses in the Venturi geometry, we have performed and analysed the unsteady kinetic energy balance (Bernoulli's equation) in the flow:

$$-P_f = \int_D \left\{ \frac{\partial}{\partial t}\left(\frac{\rho \vec{V}^2}{2}\right) - p\,div\vec{V} \right\} dV + \int_S \left(\frac{\rho \vec{V}^2}{2} + p\right) \vec{V}.\vec{n}\,dS$$

where P_f is the instantaneous power dissipated by viscous shear.

The term $\int_D \left\{ \frac{\partial}{\partial t}\left(\frac{\rho \vec{V}^2}{2}\right) \right\} dV$ corresponds to kinetic energy fluctuation; the term $\int_S \left(\frac{\rho \vec{V}^2}{2} + p\right) \vec{V}.\vec{n}\,dS$ corresponds to surface convective flux; the term $\int_D \{ -p\,div\vec{V} \} dV$ corresponds to compressibility effects.

Results obtained in cases 1 and 5 (see Figures 20) show that the term corresponding to compressibility effects is negligible. The instantaneous dissipated power P_f is given by the difference between surface convective flux and kinetic energy variation.

According to these results, the head losses decrease during the attached cavitation sheet increase (Figures 21). The minimal value of P_f takes place when the attached sheet cavitation is broken by the re-entrant jet. Then, head losses begin to enhance. The head losses continue to increase during the convection of shed cloud structure. The maximal head losses occur when no attached sheet is observed at the Venturi throat.

The fluctuations of the head losses simulated by the barotropic model are more relevant than ones calculated by the vapour ratio transport equation. As observed during vapour volume variation analyses, the global behaviour of head losses fluctuations obtained by the barotropic model is more irregular.

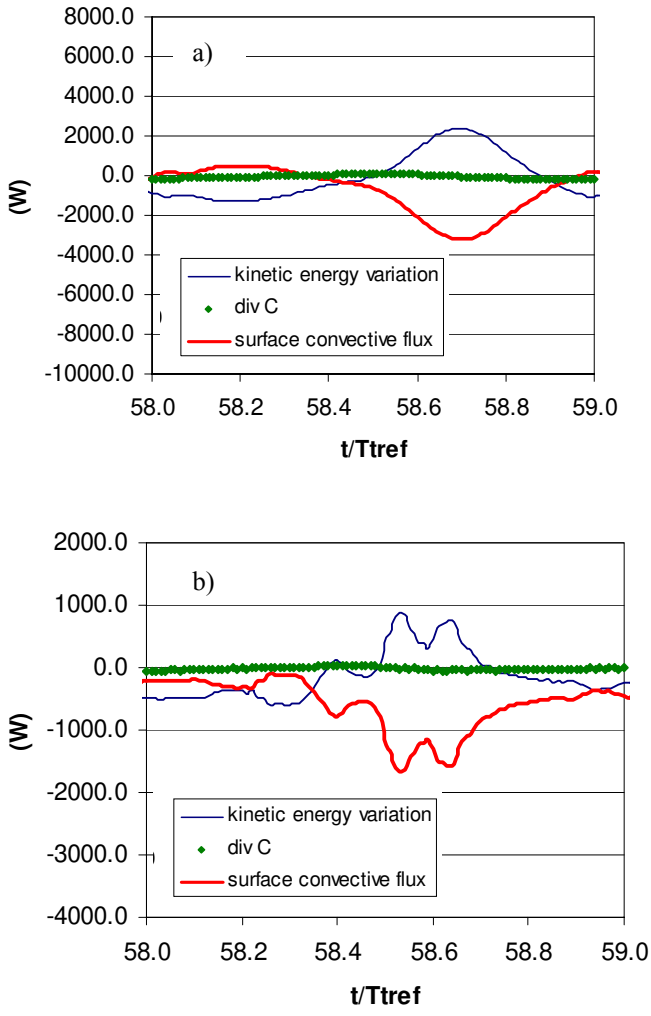

Figure 20: Bernoulli's equation balance: results obtained for a) case 5 and b) case 1 during a cloud shedding period.

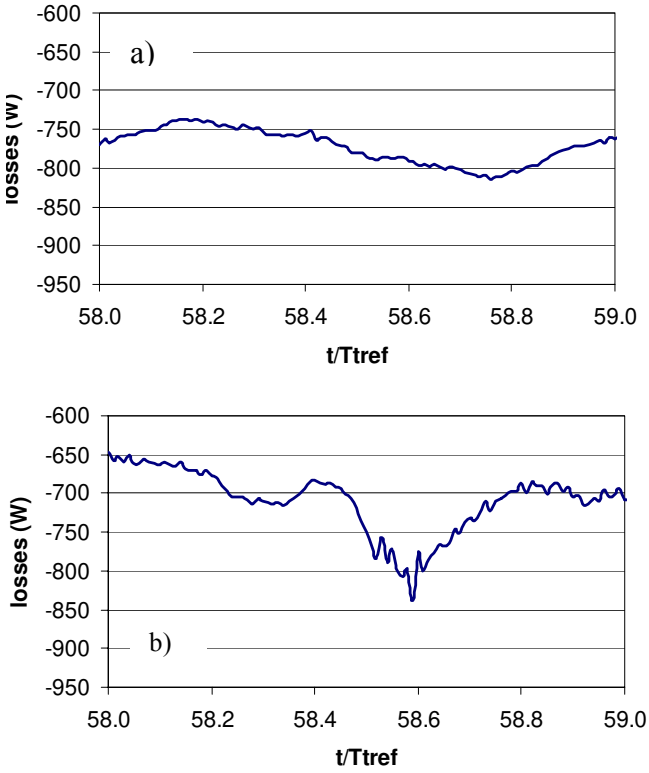

Figure 21: Dissipated power P_f
Results obtained for a) case 5 and b) case 1 during a cloud shedding period.

CONCLUSION

A quite complete study of an instable cavitation sheet in a 2D Venturi configuration was performed by experimental and numerical approaches. Compared to previous works done in the same geometry, some important improvements both on the experimental method and data processing algorithms were carried out to obtain more precise and reliable results concerning void ratio and instantaneous velocity fields.

About numerical aspects, the cavitating unsteady code "IZ" was modified, allowing the application and the comparisons between two different physical approaches, i.e., the barotropic and the void ratio equation transport models. Several numerical tests were performed to study the influence of physical parameters.

Results show that the performed numerical simulations were able to describe qualitatively the unsteady behaviour of the cavitation sheet. A global analysis of the sheet pulsation cycle was performed and provided acceptable results. Nevertheless, by performing a local and unsteady analysis of the void ratio and velocity fields, the study showed that there is no global agreement between all the computations done, mainly concerning void ratio distribution inside the attached cavitation sheet.

A special analysis of the unsteady statistics behaviour of the velocity field was also made for a particular location in the flow (Y=2mm at station 1). This approach clearly showed that, even when a good agreement is obtained for time averaged values, some very high discrepancies exist in the statistical structure of the velocity fluctuations. This may result in different scenarios to describe dynamics of the flow. This effect will be studied more extensively in the near future by performing a phase averaging analysis of both numerical and experimental data to describe completely the velocity field dynamics.

The original experimental/numerical coupled approach proposed in this paper appears to be a useful tool to analyse and characterize unsteady cavitating flows.

ACKNOWLEDGMENTS

The authors wish to express their gratitude to the French space agency CNES and to the SNECMA company for their continuous support.

REFERENCES

Coutier-Delgosha O., Fortes-Patella R., Reboud J-L., (2002), "Simulation of unsteady cavitation with a two-equations turbulence model including compressibility effects", J. of Turbulence, Vol. 3, 058, http:\\jot.iop.org.

Coutier-Delgosha O., Reboud J-L., Delannoy Y. (2003a), "Numerical simulation of the unsteady behaviour of cavitating flows", Int. J. for Numerical Meth. In fluids, Vol. 42, pp. 527-548.

Coutier-Delgosha O., Fortes-Patella, R., Reboud J.L. (2003b), "Evaluation of the turbulence model influence on the numerical simulations of unsteady cavitation", J of Fluids Eng., Vol. 125 pp. 38-45.

Coutier-Delgosha O., Fortes-Patella R., Reboud J.-L., Stutz B. (2004) "test case no 30: unsteady cavitation in a venturi type section", Multiphase Science and Technology, Vol. 16, Nos. 1-3, pp. 205-215, 2004.

Delannoy Y., Kueny J.L. (1990), "Two phase flow approach in unsteady cavitation modelling", Cavitation and Multiphase Flow Forum, ASME-FED vol 98, pp 153-158.

Fortes-Patella R., Coutier-Delgosha O., Perrin J., Reboud J-L., (2006), "A numerical model to predict unsteady cavitating flow behaviour in inducer blade cascades", to be published in Journal of Fluid Engineering.

Kunz, R., Boger, D., Chyczewski, T., Stinebring, D., Gibeling, H. (1999), "Multi-phase CFD analysis of natural and ventilated cavitation about submerged bodies", ASME FEDSM 99-7364, San Francisco.

Lohrberg H., Stoffel B., Fortes-Patella R., Coutier-Delgosha O. Reboud JL. (2002) : "Numerical and Experimental Investigations on the Cavitating Flow in a Cascade of Hydrofoils", Experiments in Fluids, 33/4 : pp 578-586.

Longatte, F. (1998), "Contribution à l'Analyse Phénoménologique des Ecoulements Instationnaires dans les Turbomachines: Etude du Couplage Pompe-Circuit et Rotor-Stator", Ph.D. Thesis, INPGrenoble, France.

Patankar S.V., (1981), *Numerical Heat Transfer and Fluid Flow*, Hemisphere Publishing Corporation.

Pouffary B., Fortes-Patella R., Reboud J.L., (2004) : "Unsteady cavitating flows in turbomachinery: comparison of two numerical models and applications", Proceedings of

ECCOMAS2004 Symposium, Invited lecture, July 2004, Finland.

Reboud J-L., Stutz B. and Coutier O. (1998), “Two-phase flow structure of cavitation : experiment and modelling of unsteady effects”, 3rd Int. Symp. on Cavitation, Grenoble, France, April 1998.

Reboud, JL., Fortes-Patella, R., Hofmann, M., Lohrberg, H., Ludwig, G., Stoffel, B. (1999), "Numerical and experimental investigations on the self-oscillating behavior of cloud cavitation", ASME-FEDSM 99-6755/7259, San Francisco.

Reboud J-L., Coutier O., Pouffary B., Fortes-Patella R. (2003) : "Numerical simulations of unsteady cavitating flows: some applications and open problems", *Proceedings of CAV 2003 Symposium*, Conférence Invitée, November 2003, Osaka.

Rolland J., Boitel G., Barre S., Fortes Patella R. (2006), “Experiments and modelling of cavitating flows in Venturi, Part I: stable cavitation”, *Sixth International Symposium on Cavitation, CAV2006*, Wageningen, The Netherlands, September 2006.

Rossi S. (2004), “Etude expérimentale des écoulements instationnaires cavitants: application au cas d’un Venturi bidimensionnel ”, Master report, Laboratoire des Ecoulements Géophysiques et Industriels, June 2004.

Stutz B., “Analyse de la structure diphasique et instationnaire de poches de cavitation” (1996), Ph. D. Thesis, INPG, CREMHYG Laboratory.

Stutz B., Reboud J.L. (1997a), “Two-phase flow structure of sheet cavitation”, Phys. Fluids vol 9 (12) pp 3678-3686.

Stutz B., Reboud J.L. (1997b), “Experiments one unsteady cavitation”, Exp. In Fluids, Flight. 22, pp 191-198.

Stutz B., Reboud J.L. (2000), “Measurements within unsteady cavitation”, Experiments in Fluids, n°29, pp 545-552.

Stutz B. (2003), “Influence of Roughness one the Two-Phase Flow Structure of Sheet Cavitation”, J of Fluids Eng., vol. 125, pp 652-659.

Thompson K.W. (1987), “Time dependent boundary conditions for hyperbolic systems”, Journal of Computational Physics, Vol. 68, pp. 1-24.

Thompson K.W. (1990), “Time dependent boundary conditions for hyperbolic systems, Part II”, Journal of Computational Physics, Vol. 89, pp. 439-461.

Zhu J. (1991), "A low diffusive and oscillation-free convection scheme", Comm. in Applied Num. Methods, vol. 7.